crystals

MDPI

*Article*

# The Face-to-Face σ-Hole···σ-Hole Stacking Interactions: Structures, Energies, and Nature

**Yu Zhang and Weizhou Wang ***

Henan Key Laboratory of Function-Oriented Porous Materials, College of Chemistry and Chemical Engineering, Luoyang Normal University, Luoyang 471934, China; yzhpaper@yahoo.com
* Correspondence: wzw@lynu.edu.cn; Tel.: +86-379-686-18320

**Abstract:** The existence of the π···π stacking interaction is well-known. Similarly, it is reasonable to assume the existence of the σ-hole···σ-hole stacking interaction. In this work, the structures, energies, and nature of the face-to-face σ-hole···σ-hole stacking interactions in the crystal structures have been investigated in detail by the quantum chemical calculations. The calculated results clearly show that the face-to-face σ-hole···σ-hole stacking interactions exist and have unique properties, although their strengths are not very significant. The energy component analysis reveals that, unlike many other dispersion-dominated noncovalent interactions in which the induction energies always play minor roles for their stabilities, for the face-to-face σ-hole···σ-hole stacking interaction the contribution of the induction energy to the total attractive energy is close to or even larger than that of the electrostatic energy. The structures, energies, and nature of the face-to-face σ-hole···σ-hole stacking interactions confined in small spaces have also been theoretically simulated. One of the important findings is that encapsulation of the complex bound by the face-to-face σ-hole···σ-hole stacking interaction can tune the electronic properties of the container.

**Keywords:** face-to-face; σ-hole···σ-hole stacking interaction; PBE0-D3(BJ) calculation; energy component analysis; confined σ-hole···σ-hole stacking interaction



**Citation:** Zhang, Y.; Wang, W. The Face-to-Face σ-Hole···σ-Hole Stacking Interactions: Structures, Energies, and Nature. *Crystals* **2021**, *11*, 877. https://doi.org/10.3390/cryst11080877

Academic Editor: Antonio Frontera

Received: 10 July 2021
Accepted: 26 July 2021
Published: 28 July 2021



## 1. Introduction

Science and engineering are now in the era of the molecule. Naturally, the study of intermolecular interactions is the core of molecular science and engineering. There have been many different types of intermolecular interactions. Especially in recent years, many new terms and concepts have been introduced in order to describe intermolecular interactions more accurately [1–15]. The σ bond and π bond are two most common and important chemical bonds. The existence of the π···π stacking interaction (also called the aromatic–aromatic interaction or aromatic stacking interaction) is well-known. Similarly, it is reasonable to assume the existence of the σ-hole···σ-hole stacking interaction [15].

Unlike the halogen bond or the other σ-hole bond, in which the electrophilic region of a σ-hole points to the nucleophilic region in another or the same molecular entity [16,17], the σ-hole···σ-hole stacking interaction is the net attractive interaction between two σ-hole regions with the similar electron-density distributions. Figure 1 is a simple schematic diagram of four different kinds of the σ-hole···σ-hole stacking interactions. In the Cambridge Structural Database (Version 5.42, February 2021) [18], the edge-to-edge σ-hole···σ-hole stacking interactions shown in Figure 1 are seldom found. Hence, in this study, we only focused on the face-to-face σ-hole···σ-hole stacking interactions. Let us stress here that the use of the term "σ-hole···σ-hole stacking interaction" is reasonable because the two σ-holes with similar electron-density distributions are stacked with each other, which leads to the stacking of the two σ bonds and further the stacking of the two molecules. Evidently, the σ-hole···σ-hole stacking interaction is totally different from the halogen···halogen or chalcogen···chalcogen interaction. The σ-hole···σ-hole stacking interaction is defined according to the electron-density distribution, whereas the halogen···halogen or

chalcogen· · · chalcogen interaction is judged in terms of the molecular geometries. It is also unsuitable to use the term "like-charge interaction" to describe such kind of net attractive interaction because the charge is neither a physical observable nor a strict mathematical formulation and many atoms in the molecules have both the negative electrostatic potential region and positive electrostatic potential region.

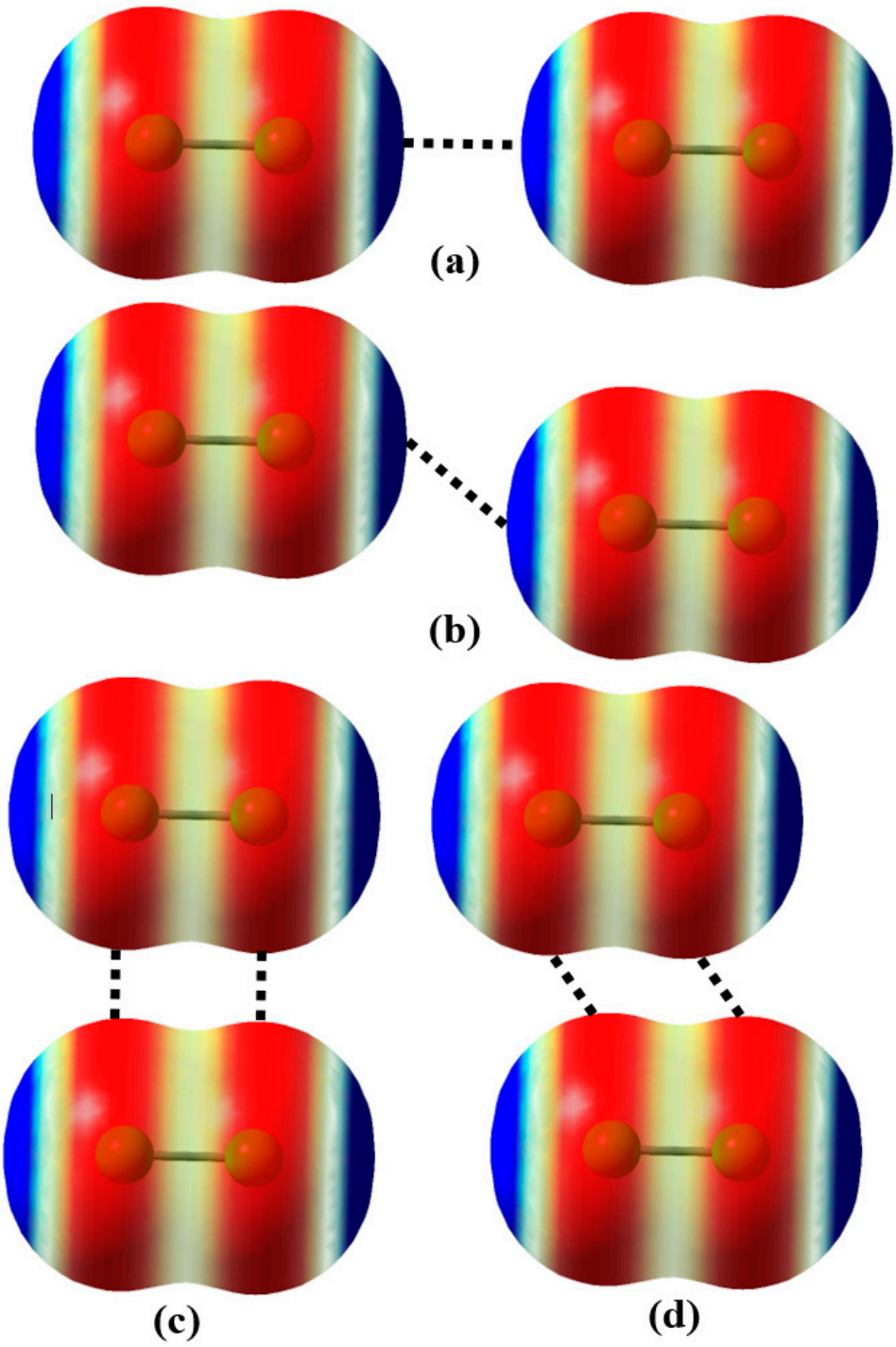


**Figure 1.** Schematic diagram of the perfect face-to-face (**a**), parallel-displaced face-to-face (**b**), perfect edge-to-edge (**c**), and parallel-displaced edge-to-edge (**d**) σ· · · σ stacking interactions. The blue surfaces represent the electrophilic regions, and the red surfaces are the nucleophilic regions.

In a previous study, we explored the structures, energies, and nature of the face-to-face σ-hole(I)· · · σ-hole(I) and σ-hole(S)· · · σ-hole(S) stacking interactions [15]. It was found that

the strengths of the face-to-face σ-hole(I)· · · σ-hole(I) and σ-hole(S)· · · σ-hole(S) stacking interactions are not very large (about 1 kcal/mol). The interaction energies of the face-to-face σ-hole(I)· · · σ-hole(I) and σ-hole(S)· · · σ-hole(S) stacking interactions were calculated with the supermolecule method. Therefore, one may suspect that such small stabilization energies maybe originate from the dispersion interactions between the other parts of the complexes except for the two I(S) atoms and not from the face-to-face σ-hole· · · σ-hole stacking interactions. To settle this issue, we revisited the existence and uniqueness of the face-to-face σ-hole· · · σ-hole stacking interactions by exploring the structures, energies, and nature of the face-to-face σ-hole(Br)· · · σ-hole(Br) stacking interactions in the crystal structures of 1,6-dibromo-11,12-dimethyl-tricyclo(4.4.2.$0^{2,7}$)dodec-11-ene (refcode DASKOX), 10,10′-dibromo-9,9′-bianthryl (refcode ENIVEC), 1-bromotriptyeene (refcode BTRPYC) and triphenylbromomethane (refcode TPHMBR02) [19–22]. The other important question raised is, "Can the face-to-face σ-hole· · · σ-hole stacking interactions be observed in the gas and liquid phases?" In order to answer this question, we studied the structures, energies, and nature of the face-to-face σ-hole· · · σ-hole stacking interactions in the confined nanospace by selecting the $C_{30}$-capped armchair (5,5) carbon nanotube ($C_{120}$) as a container.

## 2. Computational Details

Unless otherwise stated, the geometries of the monomers and dimers considered in this study were taken directly from their corresponding crystal structures. As suggested by Politzer and co-workers, the molecular electrostatic potential maps of the monomers were generated by calculating the electrostatic potentials on the molecular surfaces with the 0.001 au contour of the electronic density [23]. The electrostatic potentials of the monomers and interaction energies of the dimers were calculated at the PBE0-D3(BJ)/def2-TZVPP theory level with the Gaussian 09 suite of programs [24–28]. The basis set superposition error was eliminated using the conventional counterpoise method [29]. It has been proven that the PBE0-D3(BJ)/def2-TZVPP calculations can give us accurate interaction energies of weakly bound complexes [30–33]. The atoms in molecules (AIM) theory was employed to study the nature of the σ-hole· · · σ-hole stacking interaction [34]. The AIM analysis was carried out with the AIM2000 code [35].

The energy component analyses of the total interaction energies were performed with the spin-component scaled zeroth-order symmetry-adapted perturbation theory (SCS-SAPT0) programmed in the PSI4 software package [36–39]. Our previous studies have shown that the inexpensive SCS-SAPT0 method in conjugation with the basis set aug-cc-pVDZ performs very well for the energy decomposition analyses of the π-stacked complexes [30–32]. Note that for the hydrogen-bonded or halogen-bonded complexes, the SCS-SAPT0 method maybe have a relatively poor performance [40].

## 3. Results and Discussion

### *3.1. Structures and Interaction Energies*

The crystal structures of DASKOX, ENIVEC, BTRPYC, and TPHMBR02 can be obtained from the Cambridge Structural Database. For simplicity, we used the refcode-M to name the monomers in the crystal structures and refcode-D to name the dimers in the crystal structures.

Figure 2 shows the PBE0-D3(BJ)/def2-TZVPP molecular electrostatic potential maps of the monomers DASKOX-M, ENIVEC-M, BTRPYC-M, and TPHMBR02-M. The existence of the σ-hole of the Br atom in each monomer is very clear. As pointed out earlier by Politzer and Murray, the σ-hole is a region of lower electronic density on the extension of a σ bond and it is incorrect to assume that a σ-hole has only the positive electrostatic potentials [41]. Therefore, the σ-holes of the Br atoms can be either negative or positive. Both the negative and positive σ-holes can be seen in Figure 2, although the absolute values of the surface maxima of the σ-holes of the Br atoms in DASKOX-M and TPHMBR02-M are not very large.

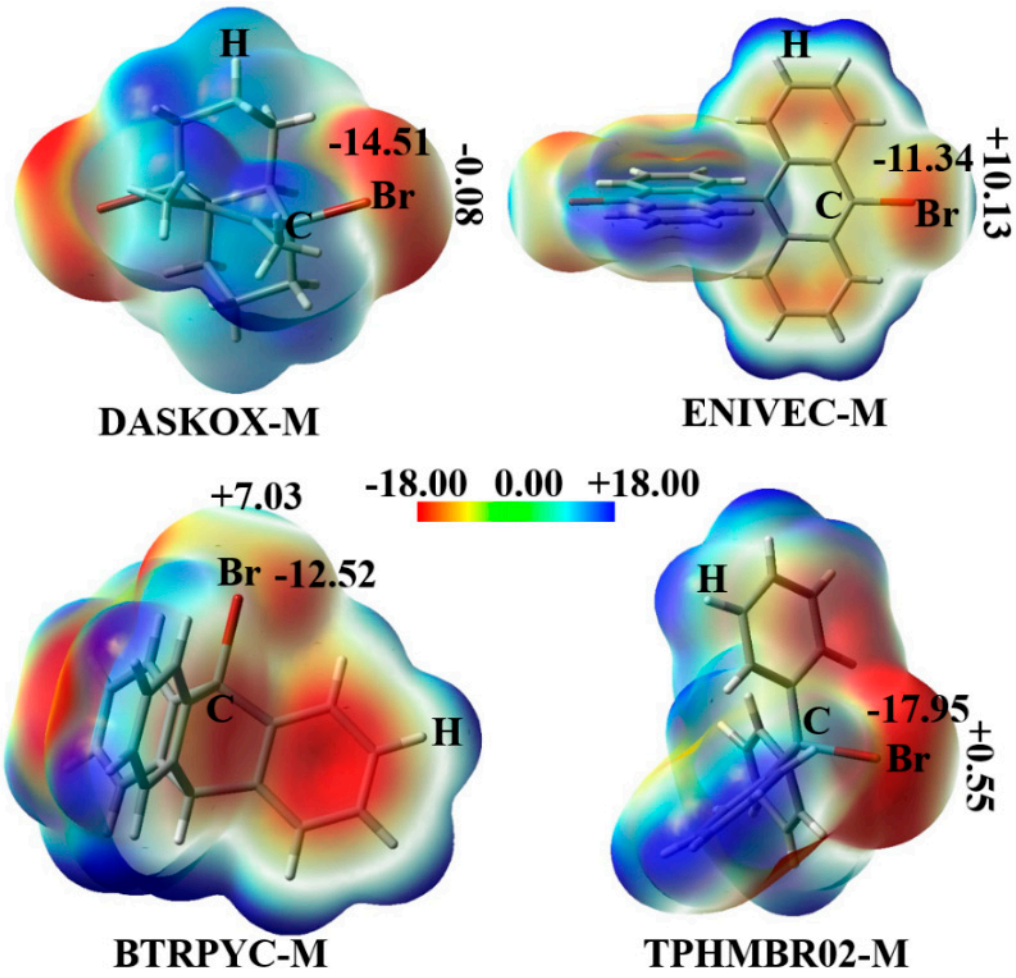


**Figure 2.** Molecular electrostatic potential maps of the monomers DASKOX-M, ENIVEC-M, BTRPYC-M, and TPHMBR02-M. The values (kcal/mol) are the surface minima and surface maxima of the σ-holes of the Br atoms.

Figure 3 demonstrates the geometries and interaction energies of the dimers DASKOX-D, ENIVEC-D, BTRPYC-D, and TPHMBR02-D. Also shown in Figure 3 are the one-dimensional chain structures formed by the face-to-face σ-hole(Br)$\cdots$σ-hole(Br) stacking interactions in the crystal structures of DASKOX and ENIVEC. The values of the angles in Figure 3 are in the range of 174° to 180°, which indicates nearly face-to-face orientations of these σ-holes. This is a necessary condition for the formation of the face-to-face σ-hole(Br)$\cdots$σ-hole(Br) stacking interaction. The van der Waals radius of the Br atom is 1.85 Å [42]. The $Br_1\cdots Br_2$ distances in Figure 3 are all less than the sum of the van der Waals radii of two Br atoms. What we want to stress here is that the much smaller $Br_1\cdots Br_2$ distance is not a necessary condition for the formation of the face-to-face σ-hole(Br)$\cdots$σ-hole(Br) stacking interaction. At the same time, it is also noticed from Figure 3 that the $Br_1\cdots Br_2$ distance does not correlate with the interaction energy. Among the four dimers, the $Br_1\cdots Br_2$ distance in TPHMBR02-D is the smallest one, while the interaction energy of TPHMBR02-D is neither the biggest nor the smallest. The interaction energies of the four dimers are in the range of −1.29 to −0.91 kcal/mol. The strength of the face-to-face σ-hole(Br)$\cdots$σ-hole(Br) stacking interaction is comparable to that of the face-to-face σ-hole(I)$\cdots$σ-hole(I) or σ-hole(S)$\cdots$σ-hole(S) stacking interaction [15]. Although here we only focused on the face-to-face σ-hole$\cdots$σ-hole stacking interactions in the crystal structures, one may want to know whether the geometries and interaction energies of these face-to-face σ-hole$\cdots$σ-hole stacking interactions will change significantly in the gas phase.

Selecting the BTRPYC-D as a model dimer, we fully optimized its geometries and calculated its interaction energy at the PBE0-D3(BJ)/def2-TZVPP theory level. It was found that in the gas phase the $Br_1 \cdots Br_2$ distance is 3.660 Å and the interaction energy is −1.30 kcal/mol, which are almost the same as the corresponding ones in the crystal structure.

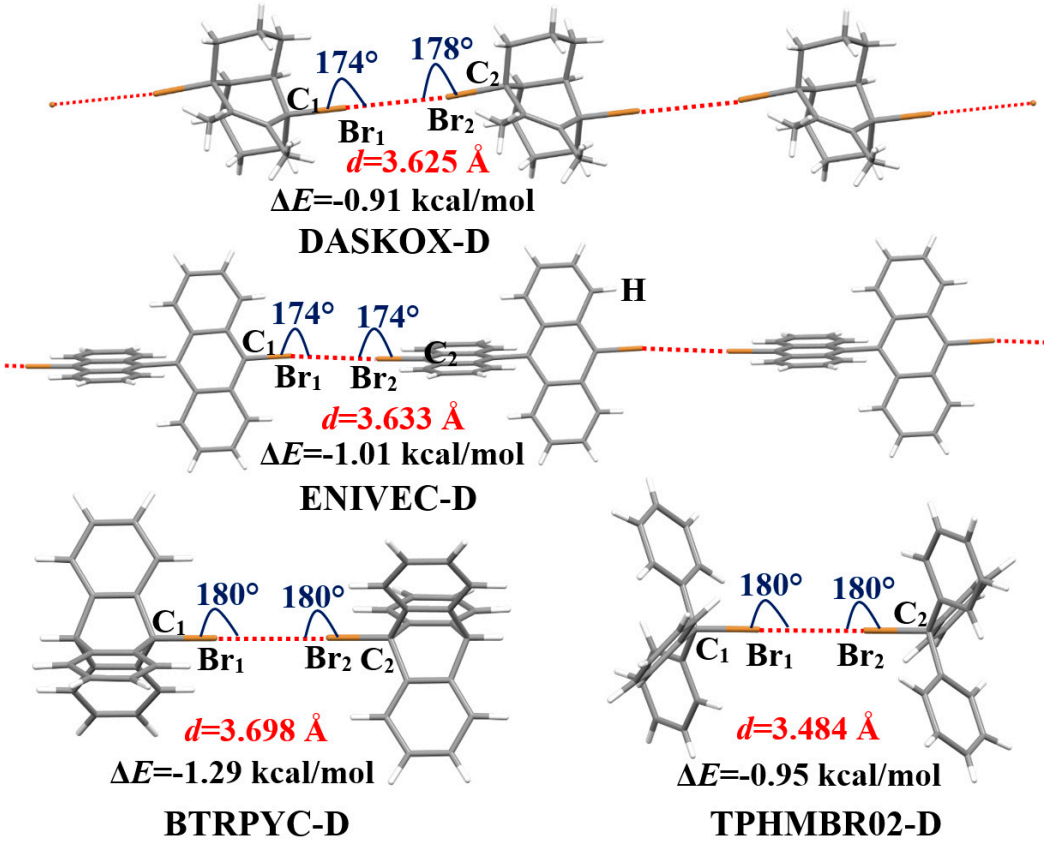


**Figure 3.** The geometries and interaction energies of the dimers DASKOX-D, ENIVEC-D, BTRPYC-D, and TPHMBR02-D.

The small stabilization energies and large dimers with more than 68 atoms will make us suspect that the stabilization energies maybe originate from the dispersion interactions between the other parts of the dimers except for the two Br atoms and not from the unique σ-hole(Br)$\cdots$σ-hole(Br) stacking interactions. In order to clear up the doubt, we replaced the Br atoms in the four dimers with the H atoms and recalculated the interaction energies of the corresponding dimers. The C-H bond length is kept constant at 1.07 Å, and the geometries of other parts of the dimers except for the Br atoms are kept unchanged. At the PBE0-D3(BJ)/def2-TZVPP level of theory, the interaction energies are −0.12, −0.13, −0.20, and −0.33 kcal/mol for the H-replaced DASKOX-D, ENIVEC-D, BTRPYC-D, and TPHMBR02-D, respectively. The H$\cdots$H distances in the four H-replaced dimers are all larger than 5.27 Å. Such large intermolecular distances result in the fact that the electrostatic, exchange, and induction energies are all very small and can be neglected. Hence, the PBE0-D3(BJ)/def2-TZVPP interaction energies can be regarded as the dispersion energies between the other parts of the dimers except for the Br atoms. Evidently, the absolute values of these interaction energies are much smaller than the corresponding ones for the dimers DASKOX-D, ENIVEC-D, BTRPYC-D, and TPHMBR02-D, which proves that the stabilization energies of the four dimers are dominated by the face-to-face σ-hole(Br)$\cdots$σ-hole(Br) stacking interactions and not by the dispersion interactions between the other parts of the dimers except for the two Br atoms.

The sum of the van der Waals radii of the Br and H atoms is 3.05 Å [42]. The Br$\cdots$H interatomic distances in Figure 3 are all larger than 5.18 Å. The much larger interatomic distances means that the Br$\cdots$H interactions in the dimers DASKOX-D, ENIVEC-D, BTRPYC-

D, and TPHMBR02-D should be very weak and can also be neglected. Again, it is proved that the stabilization energies of these dimers only originate from the unique σ-hole(Br)$\cdots$σ-hole(Br) stacking interactions. In fact, compared with the other noncovalent interactions such as the halogen bonds and $\pi\cdots\pi$ stacking interactions, the σ-hole$\cdots$σ-hole stacking interactions are much purer because the accompanying intermolecular secondary interactions are all negligible due to the much larger intermolecular distances caused by the two linear σ bonds.

### *3.2. Energy Component Analysis*

The results of the energy component analyses for the dimers DASKOX-D, ENIVEC-D, BTRPYC-D, and TPHMBR02-D are summarized in Table 1. The total interaction energy ($E_{tot}$) and its energy components electrostatic ($E_{elst}$), exchange ($E_{exch}$), induction ($E_{ind}$), and dispersion ($E_{disp}$) energies were calculated at the SCS-SAPT0/aug-cc-pVDZ theory level. Here, the total interaction energies are comparable to the corresponding ones calculated at the PBE0-D3(BJ)/def2-TZVPP level of theory, which again indicates the reliability of the SCS-SAPT0/aug-cc-pVDZ calculations.

**Table 1.** The energy component analyses for the four dimers. All energies are in kcal/mol.

| Energy Component | DASKOX-D | ENIVEC-D | BTRPYC-D | TPHMBR02-D |
|---|---|---|---|---|
| $E_{tot}$ | −0.95 | −1.24 | −1.59 | −1.19 |
| $E_{elst}$ | −0.41 | −0.25 | −0.41 | −0.61 |
| $E_{exch}$ | 1.96 | 1.29 | 1.13 | 3.01 |
| $E_{ind}$ | −0.43 | −0.41 | −0.31 | −0.81 |
| $E_{disp}$ | −2.07 | −1.87 | −2.00 | −2.79 |
| $E_{elst}$% [a] | 14% | 10% | 15% | 15% |
| $E_{ind}$% [a] | 15% | 16% | 11% | 19% |
| $E_{disp}$% [a] | 71% | 74% | 74% | 66% |

[a] The percentage in the total attractive interaction energy.

The contribution of each energy component to the total attractive energy can be clearly seen in Table 1. The dispersion energies contribute about 70% of the total attractive interaction energies. This means that the face-to-face σ-hole(Br)$\cdots$σ-hole(Br) stacking interactions are dispersion-dominated, which is in good agreement with previous finding for the σ-hole(I)$\cdots$σ-hole(I) and σ-hole(S)$\cdots$σ-hole(S) stacking interactions [15]. The electrostatic energies and induction energies contribute 10% to 19% of the total attractive interaction energies. Unlike the other dispersion-dominated complexes in which the electrostatic energies always play secondary roles for their stabilities, here in the four dimers the contribution of the induction energy to the total attractive energy is close to or even larger than that of the electrostatic energy. Figure 4 shows the correlation of the induction energies with the interatomic distances. The values of the Pearson's correlation coefficient, coefficient of determination, and adjusted correlation coefficient are all close to 1.00. Evidently, there is a strong correlation between the induction energy and the interatomic distance. The absolute values of the induction energies are inversely proportional to the $Br_1\cdots Br_2$ interatomic distances. In Table 1, the contribution of the induction energy to the total attractive interaction energy of the dimer BTRPYC-D is the smallest one and the contribution of the induction energy to the total attractive interaction energy of the dimer TPHMBR02-D is the largest one. This is reasonable because the $Br_1\cdots Br_2$ distance in the dimer BTRPYC-D is the longest one and the $Br_1\cdots Br_2$ distance in the dimer TPHMBR02-D is the shortest one.

As shown in the third row of Table 1, the electrostatic terms are all attractive, which seems contradictory to the fact that the two face-to-face σ-holes have the same electron-density distributions. At the same time, it is noticed that the electrostatic energies in Table 1 do not correlate with the most positive potentials of the σ-holes in Figure 2. On the other hand, unlike the induction energies, the electrostatic energies do not correlate with the $Br_1\cdots Br_2$ interatomic distances. In fact, such cases have been widely found in

the study of the π···π stacking interactions [43]. Sherrill and coworkers have pointed out that the charge penetration is the cause of these counterintuitive effects [43]. The charge penetration effects play key roles for understanding the electrostatic components of both π···π stacking interactions and σ-hole···σ-hole stacking interactions.

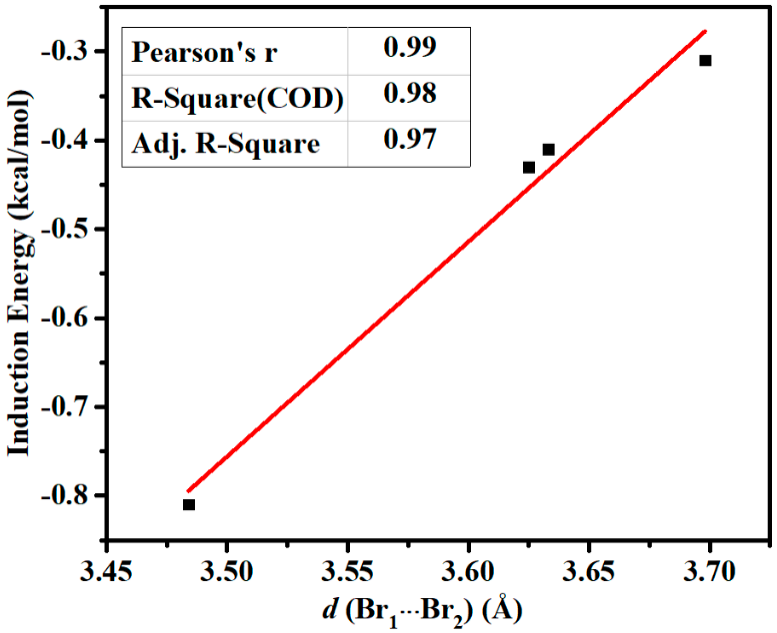


**Figure 4.** The correlation of the induction energies with the interatomic distances.

### *3.3. AIM Analysis*

To further explore the nature of the σ-hole···σ-hole stacking interaction, AIM analysis has also been carried out for the four dimers DASKOX-D, ENIVEC-D, BTRPYC-D, and TPHMBR02-D. The AIM theory is based on a topological analysis of the electron charge density and its Laplacian. Figure 5 shows the molecular graphs with the values of electron densities and their corresponding Laplacians at the bond critical points of the $Br_1 \cdots Br_2$ contacts for the dimers DASKOX-D, ENIVEC-D, BTRPYC-D, and TPHMBR02-D. For clarity, only the bond critical points are shown and the ring critical points are omitted. The values of the electron densities at the bond critical points of the $Br_1 \cdots Br_2$ contacts range from 0.0049 to 0.0079 au, and the values of their corresponding Laplacians range from 0.0182 to 0.0270 au. According to Bader's AIM theory, for the closed-shell interactions (van der Waals interactions, hydrogen bonds, and ionic bonds), the values of the electron densities at the bond critical points are relatively small and their corresponding Laplacians are positive [34]. Evidently, the $Br_1 \cdots Br_2$ contacts in the dimers DASKOX-D, ENIVEC-D, BTRPYC-D, and TPHMBR02-D are all of the noncovalent interactions. As shown in Figure 5, except for the σ-hole(Br)···σ-hole(Br) stacking interactions, there are no other noncovalent interactions in the four dimers. Being consistent with the conclusions in Section 3.1, the results of the AIM analyses also rule out the possible effects of other noncovalent interactions.

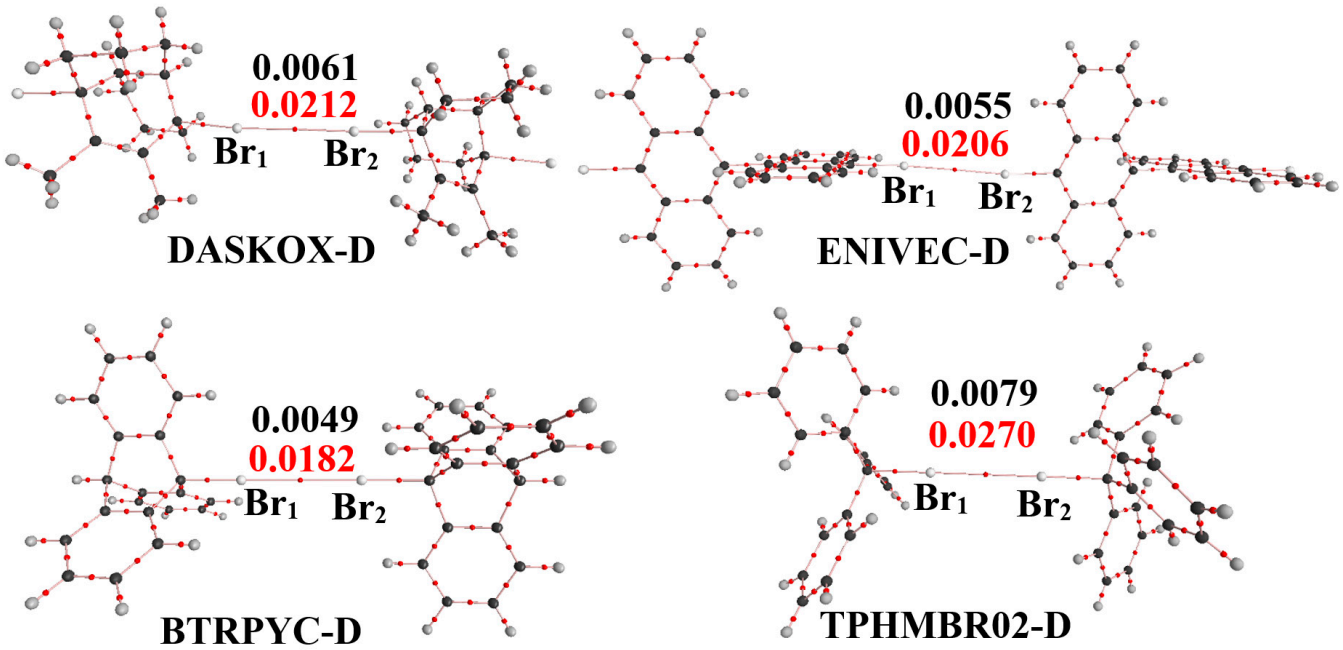


**Figure 5.** The electron densities (black numbers, au) and their corresponding Laplacians (red numbers, au) at the bond critical points (small red dots) of the $Br_1 \cdots Br_2$ contacts in the dimers DASKOX-D, ENIVEC-D, BTRPYC-D, and TPHMBR02-D.

### *3.4. Confinement of the Face-to-Face σ-Hole···σ-Hole Stacking Interaction*

The configurations of the complexes bound by the face-to-face σ-hole···σ-hole stacking interactions are obviously not the global minima on the potential energy surfaces. Hence, an important and interesting question is whether the face-to-face σ-hole···σ-hole stacking interactions can be observed in the gas and liquid phases. One possibility to observe the existence of the face-to-face σ-hole···σ-hole stacking interaction in the gas or liquid phase is to encapsulate the complex bound by the face-to-face σ-hole···σ-hole stacking interaction into a container [44,45]. Here, we selected the $C_{120}$ as a model container and the face-to-face $Br_2 \cdots Br_2$ as a model dimer to simulate such a case. Note that, in the organic solutions, many single-molecule or self-assembled capsules have been reported [44,45].

Figure 6 shows the optimized configurations, the highest occupied molecular orbital (HOMOs), and the lowest unoccupied molecular orbitals (LUMOs) of $Br_2$, $Br_2 \cdots Br_2$, and $(Br_2 \cdots Br_2)@C_{120}$. Table 2 summarizes the Br-Br bond lengths, $Br \cdots Br$ interatomic distances, formation free energies, HOMO energies, LUMO energies, and LUMO–HOMO energy gaps, of $Br_2$, $Br_2 \cdots Br_2$, and $(Br_2 \cdots Br_2)@C_{120}$, calculated at the PBE0-D3(BJ)/def2-TZVPP level of theory. The optimized Br-Br bond length of $Br_2$ is 2.2817 Å, which is in excellent agreement with the experimental value of 2.2811 Å [46]. The Br-Br bond length becomes much longer upon the formation of $(Br_2 \cdots Br_2)@C_{120}$. The $Br \cdots Br$ interatomic distance is 3.8296 Å in the dimer $Br_2 \cdots Br_2$ and becomes much shorter as the dimer $Br_2 \cdots Br_2$ is encapsulated into $C_{120}$. The face-to-face configuration of $Br_2 \cdots Br_2$ is not the local or global minimum on the potential energy surface, which is consistent with its positive formation free energy. However, $(Br_2 \cdots Br_2)@C_{120}$ is quite stable, and its formation free energy is −77.84 kcal/mol. This means that, even in the gas or liquid phase, the face-to-face σ-hole···σ-hole stacking interactions can be easily observed in the complexes confined in small spaces.

As can be seen in Table 2, the LUMO–HOMO energy gap decreases slightly from 4.59 eV to 4.13 eV upon the dimer $Br_2 \cdots Br_2$ formation, and the LUMO–HOMO energy gap decreases sharply from 4.13 eV to 0.92 eV when encapsulating the dimer $Br_2 \cdots Br_2$ into the capped carbon nanotube $C_{120}$. Compared with the LUMO–HOMO energy gap of $C_{120}$ with a value of 1.61 eV, the LUMO–HOMO energy gap of $(Br_2 \cdots Br_2)@C_{120}$ is

still significantly decreased. The diagrams of frontier orbitals in Figure 6 can explain the reason why the LUMO–HOMO energy gap of $(Br_2\cdots Br_2)@C_{120}$ decreases sharply. The HOMO of $(Br_2\cdots Br_2)@C_{120}$ delocalizes over $C_{120}$, whereas the LUMO of $(Br_2\cdots Br_2)@C_{120}$ delocalizes over $Br_2\cdots Br_2$. It can be clearly seen from Table 2 that the HOMO energy of $C_{120}$ is higher than that of $Br_2\cdots Br_2$, and the LUMO energy of $Br_2\cdots Br_2$ is lower than that of $C_{120}$. Therefore, the LUMO–HOMO energy gap of $(Br_2\cdots Br_2)@C_{120}$ is lower than that of both $Br_2\cdots Br_2$ and $C_{120}$. Evidently, encapsulation of $Br_2\cdots Br_2$ into $C_{120}$ tunes the electronic properties of $C_{120}$. Here, it must be stressed that the $C_{30}$-capped armchair (5,5) carbon nanotube was selected as a model container, and the results should be similar if the other capsules were used.

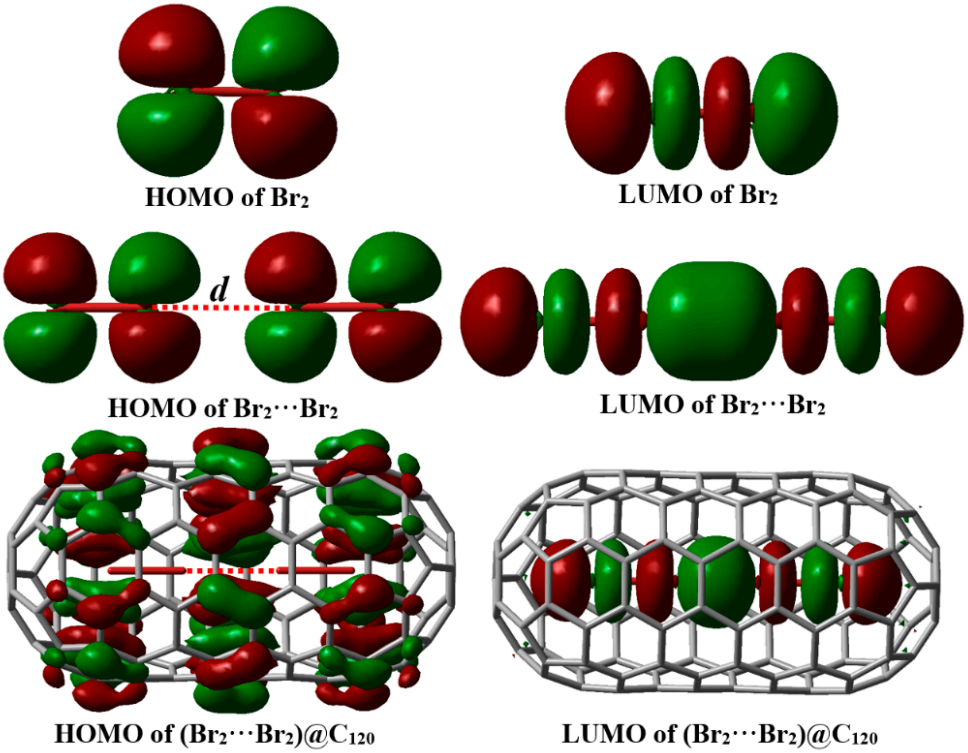


**Figure 6.** The optimized configurations and frontier orbitals of $Br_2$, $Br_2\cdots Br_2$, and $(Br_2\cdots Br_2)@C_{120}$.

**Table 2.** The bond lengths ($r$, Å), interatomic distances ($d$, Å), formation free energies ($\Delta G$, kcal/mol), HOMO energies ($E_{HOMO}$, eV), LUMO energies ($E_{LUMO}$, eV), and LUMO–HOMO energy gaps ($E_g$, eV), of $Br_2$, $Br_2\cdots Br_2$, and $(Br_2\cdots Br_2)@C_{120}$.

| | $Br_2$ | $Br_2\cdots Br_2$ | $(Br_2\cdots Br_2)@C_{120}$ |
|---|---|---|---|
| $r$ | 2.2817 (2.2811) [a] | 2.2803 | 2.2882 |
| $d$ | | 3.8296 | 3.1112 |
| $\Delta G$ | | +10.90 | −77.84 |
| $E_{HOMO}$ | −8.10 | −8.14 | −5.47 (−5.46) [b] |
| $E_{LUMO}$ | −3.51 | −4.01 | −4.55 (−3.85) [b] |
| $E_g$ | 4.59 | 4.13 | 0.92 (1.61) [b] |

[a] The experimental value. [b] The corresponding value of $C_{120}$.

## 4. Conclusions

In the present study, we have theoretically investigated the structures, energies, and nature of the face-to-face σ-hole$\cdots$σ-hole stacking interactions in the crystal structures and in the confined nanospace, respectively. The face-to-face σ-hole$\cdots$σ-hole stacking interaction is a subset of the σ-hole$\cdots$σ-hole stacking interaction, and is of the highly directional noncovalent interaction. The binding energies of the face-to-face σ$\cdots$σ stacking

interactions are generally less than 2 kcal/mol, and the dispersion forces play dominant roles for the stability of the face-to-face σ-hole$\cdots$σ-hole stacking interactions. Although single face-to-face σ-hole$\cdots$σ-hole stacking interaction may be very weak, the sum of a large number of face-to-face σ-hole$\cdots$σ-hole stacking interactions may be very strong, such as the cases in the crystal structures. Different from many other dispersion-dominated noncovalent interactions in which the induction energies always play minor roles for their stabilities, for the face-to-face σ-hole$\cdots$σ-hole stacking interaction the contribution of the induction energy to the total attractive energy is close to or even larger than that of the electrostatic energy.

The structures, energies, and nature of the face-to-face σ-hole$\cdots$σ-hole stacking interactions confined in small spaces have also been theoretically simulated. The unstable complexes bound by the face-to-face σ-hole$\cdots$σ-hole stacking interactions may become very stable as they are encapsulated into suitable containers. An important finding is that encapsulation of the complexes bound by the face-to-face σ-hole$\cdots$σ-hole stacking interactions can tune the electronic properties of the containers.

In this work, we only studied the face-to-face σ-hole$\cdots$σ-hole stacking interactions by the quantum chemical calculations. The structures, energies, and nature of the edge-to-edge σ-hole$\cdots$σ-hole stacking interactions in the gas, liquid, and solid phases are under investigation in our laboratory. We will report the results of our theoretical calculations in the near future.

**Author Contributions:** Y.Z. performed all the quantum chemical calculations; W.W. designed and supervised this project; Y.Z. and W.W. wrote and revised the paper. All authors have read and agreed to the published version of the manuscript.

**Funding:** This research was funded by the National Science Foundation of China, grant number 21773104.

**Institutional Review Board Statement:** Not applicable.

**Informed Consent Statement:** Not applicable.

**Data Availability Statement:** Data is contained within the article.

**Acknowledgments:** We thank the National Science Foundation of China for the financial support. W.W. thanks the National Supercomputing Center in Shenzhen for the computational support.

**Conflicts of Interest:** The authors declare no conflict of interest.

## References

1. Clark, T.; Hennemann, M.; Murray, J.S.; Politzer, P. Halogen Bonding: The σ-Hole. *J. Mol. Model.* **2007**, *13*, 291–296. [CrossRef] [PubMed]
2. Politzer, P.; Murray, J.S.; Clark, T. Halogen Bonding: An Electrostatically-Driven Highly Directional Noncovalent Interaction. *Phys. Chem. Chem. Phys.* **2010**, *12*, 7748–7757. [CrossRef]
3. Murray, J.S.; Lane, P.; Clark, T.; Riley, K.E.; Politzer, P. σ-Holes, π-Holes and Electrostatically-Driven Interactions. *J. Mol. Model.* **2012**, *18*, 541–548. [CrossRef] [PubMed]
4. Wang, W.; Ji, B.; Zhang, Y. Chalcogen Bond: A Sister Noncovalent Bond to Halogen Bond. *J. Phys. Chem. A* **2009**, *113*, 8132–8135. [CrossRef] [PubMed]
5. Fanfrlík, J.; Přáda, A.; Padělková, Z.; Pecina, A.; Macháček, J.; Lepšík, M.; Holub, J.; Růžička, A.; Hnyk, D.; Hobza, P. The Dominant Role of Chalcogen Bonding in the Crystal Packing of 2D/3D Aromatics. *Angew. Chem. Int. Ed.* **2014**, *53*, 10139–10142. [CrossRef]
6. Turunen, L.; Erdélyi, M. Halogen Bonds of Halonium Ions. *Chem. Soc. Rev.* **2020**, *49*, 2688–2700. [CrossRef]
7. Lu, Y.; Shi, T.; Wang, Y.; Yang, H.; Yan, X.; Luo, X.; Jiang, H.; Zhu, W. Halogen Bonding—A Novel Interaction for Rational Drug Design? *J. Med. Chem.* **2009**, *52*, 2854–2862. [CrossRef]
8. Gao, L.; Zeng, Y.; Zhang, X.; Meng, L. Comparative Studies on Group III σ-Hole and π-Hole Interactions. *J. Comput. Chem.* **2016**, *37*, 1321–1327. [CrossRef]
9. Zierkiewicz, W.; Michalczyk, M.; Wysokiński, R.; Scheiner, S. On the Ability of Pnicogen Atoms to Engage in both σ and π-Hole Complexes. Heterodimers of $ZF_2C_6H_5$ (Z = P, As, Sb, Bi) and $NH_3$. *J. Mol. Model.* **2019**, *25*, 152. [CrossRef]
10. Zahn, S.; Frank, R.; Hey-Hawkins, E.; Kirchner, B. Pnicogen Bonds: A New Molecular Linker? *Chem. Eur. J.* **2011**, *17*, 6034–6038. [CrossRef]

11. Bauzá, A.; Mooibroek, T.J.; Frontera, A. Tetrel-Bonding Interaction: Rediscovered Supramolecular Force? *Angew. Chem. Int. Ed.* **2013**, *52*, 12317–12321. [CrossRef] [PubMed]
12. Bauzá, A.; Frontera, A. Aerogen Bonding Interaction: A New Supramolecular Force? *Angew. Chem. Int. Ed.* **2015**, *54*, 7340–7343. [CrossRef] [PubMed]
13. Montero-Campillo, M.M.; Sanz, P.; Mó, O.; Yáñez, M.; Alkorta, I.; Elguero, J. Alkaline-Earth (Be, Mg and Ca) Bonds at the Origin of Huge Acidity Enhancements. *Phys. Chem. Chem. Phys.* **2018**, *20*, 2413–2420. [CrossRef] [PubMed]
14. Bauzá, A.; Alkorta, I.; Elguero, J.; Mooibroek, T.J.; Frontera, A. Spodium Bonds: Noncovalent Interactions Involving Group 12 Elements. *Angew. Chem. Int. Ed.* **2020**, *59*, 17482–17487. [CrossRef] [PubMed]
15. Zhang, Y.; Wang, W. The σ-Hole$\cdots$σ-Hole Stacking Interaction: An Unrecognized Type of Noncovalent Interaction. *J. Chem. Phys.* **2020**, *153*, 214302. [CrossRef] [PubMed]
16. Desiraju, G.R.; Ho, P.S.; Kloo, L.; Legon, A.C.; Marquardt, R.; Metrangolo, P.; Politzer, P.; Resnati, G.; Rissanen, K. Definition of the Halogen Bond. *Pure Appl. Chem.* **2013**, *85*, 1711–1713. [CrossRef]
17. Aakeroy, C.B.; Bryce, D.L.; Desiraju, G.R.; Frontera, A.; Legon, A.C.; Nicotra, F.; Rissanen, K.; Scheiner, S.; Terraneo, G.; Metrangolo, P.; et al. Definition of the Chalcogen Bond. *Pure Appl. Chem.* **2019**, *91*, 1889–1892. [CrossRef]
18. Groom, C.R.; Bruno, I.J.; Lightfoot, M.P.; Ward, S.C. The Cambridge Structural Database. *Acta Cryst.* **2016**, *B72*, 171–179. [CrossRef]
19. Doering, W.v.E.; Schmidhauser, J.C. Synthesis of Doubly Orthogonal Hexa-1,3,5-trienes: 11,12-Dimethylbicyclo[5.3.2]dodeca-1,6,11-triene. *J. Am. Chem. Soc.* **1984**, *106*, 5025–5026. [CrossRef]
20. Sarkar, M.; Samanta, A. 10,10′-Dibromo-9,9′-bianthryl. *Acta Cryst.* **2003**, *E59*, o1764–o1765. [CrossRef]
21. Palmer, K.J.; Templeton, D.H. Crystal and Molecular Structure of 1-Bromotriptyeene $BrC_{20}H_{13}$. *Acta Cryst.* **1968**, *B24*, 1048–1052. [CrossRef]
22. Dunand, A.; Gerdil, R. X-ray Structure and Crystal Packing Analysis of Triphenylbromomethane, $C_{19}H_{15}Br$. *Acta Cryst.* **1984**, *B40*, 59–64. [CrossRef]
23. Politzer, P.; Murray, J.S.; Clark, T.; Resnati, G. The σ-Hole Revisited. *Phys. Chem. Chem. Phys.* **2017**, *19*, 32166–32178. [CrossRef]
24. Adamo, C.; Barone, V. Toward Reliable Density Functional Methods without Adjustable Parameters: The PBE0 Model. *J. Chem. Phys.* **1999**, *110*, 6158–6169. [CrossRef]
25. Grimme, S.; Antony, J.; Ehrlich, S.; Krieg, H. A Consistent and Accurate Ab Initio Parametrization of Density Functional Dispersion Correction (DFT-D) for the 94 Elements H-Pu. *J. Chem. Phys.* **2010**, *132*, 154104. [CrossRef] [PubMed]
26. Grimme, S.; Ehrlich, S.; Goerigk, L. Effect of the Damping Function in Dispersion Corrected Density Functional Theory. *J. Comput. Chem.* **2011**, *32*, 1456–1465. [CrossRef]
27. Weigend, F.; Ahlrichs, R. Balanced Basis Sets of Split Valence, Triple Zeta Valence and Quadruple Zeta Valence Quality for H to Rn: Design and Assessment of Accuracy. *Phys. Chem. Chem. Phys.* **2005**, *7*, 3297–3305. [CrossRef] [PubMed]
28. Frisch, M.J.; Trucks, G.W.; Schlegel, H.B.; Scuseria, G.E.; Robb, M.A.; Cheeseman, J.R.; Scalmani, G.; Barone, V.; Mennucci, B.; Petersson, G.A.; et al. *Gaussian 09, Revision C.01*; Gaussian, Inc.: Wallingford, CT, USA, 2010.
29. Boys, S.F.; Bernardi, F. The Calculation of Small Molecular Interactions by the Difference of Separate Total Energies. Some Procedures with Reduced Errors. *Mol. Phys.* **1970**, *19*, 553–566. [CrossRef]
30. Wang, W.; Zhang, Y.; Wang, Y.B. Noncovalent $\pi\cdots\pi$ Interaction between Graphene and Aromatic Molecule: Structure, Energy, and Nature. *J. Chem. Phys.* **2014**, *140*, 094302. [CrossRef]
31. Wang, W.; Sun, T.; Zhang, Y.; Wang, Y.B. The Benzene$\cdots$Naphthalene Complex: A more Challenging System than the Benzene Dimer for newly Developed Computational Methods. *J. Chem. Phys.* **2015**, *143*, 114312. [CrossRef]
32. Wang, W.; Zhang, Y.; Wang, Y.B. Highly Accurate Benchmark Calculations of the Interaction Energies in the Complexes $C_6H_6\cdots C_6X_6$ (X = F, Cl, Br, and I). *Int. J. Quantum Chem.* **2017**, *117*, e25345. [CrossRef]
33. Li, M.M.; Wang, Y.B.; Zhang, Y.; Wang, W. The Nature of the Noncovalent Interactions between Benzene and $C_{60}$ Fullerene. *J. Phys. Chem. A* **2016**, *120*, 5766–5772. [CrossRef] [PubMed]
34. Bader, R.F.W. *Atoms in Molecules—A Quantum Theory*; Oxford University Press: Oxford, UK, 1990.
35. Biegler-König, F.; Schönbohm, J.; Bayles, D. AIM2000-A Program to Analyze and Visualize Atoms in Molecules. *J. Comput. Chem.* **2001**, *22*, 545–559.
36. Hohenstein, E.G.; Sherrill, C.D. Density Fitting and Cholesky Decomposition Approximations in Symmetry-Adapted Perturbation Theory: Implementation and Application to Probe the Nature of π-π Interactions in Linear Acenes. *J. Chem. Phys.* **2010**, *132*, 184111. [CrossRef]
37. Hohenstein, E.G.; Parrish, R.M.; Sherrill, C.D.; Turney, J.M.; Schaefer, H.F. Efficient Evaluation of Triple Excitations in Symmetry-Adapted Perturbation Theory via Second-Order Møller-Plesset Perturbation Theory Natural Orbitals. *J. Chem. Phys.* **2011**, *135*, 174017. [CrossRef]
38. Hohenstein, E.G.; Sherrill, C.D. Wavefunction Methods for Noncovalent Interactions. *WIREs Comput. Mol. Sci.* **2012**, *2*, 304–326. [CrossRef]
39. Parrish, R.M.; Burns, L.A.; Smith, D.G.A.; Simmonett, A.C.; DePrince, A.E., III; Hohenstein, E.G.; Bozkaya, U.; Sokolov, Y.A.; Di Remigio, R.; Richard, R.M.; et al. PSI4 1.1: An Open-Source Electronic Structure Program Emphasizing Automation, Advanced Libraries, and Interoperability. *J. Chem. Theory Comput.* **2017**, *13*, 3185–3197. [CrossRef]
40. Parker, T.M.; Burns, L.A.; Parrish, R.M.; Ryno, A.G.; Sherrill, C.D. Levels of Symmetry Adapted Perturbation Theory (SAPT). I. Efficiency and Performance for Interaction Energies. *J. Chem. Phys.* **2014**, *140*, 094106. [CrossRef] [PubMed]

41. Politzer, P.; Murray, J.S. σ-Hole Interactions: Perspectives and Misconceptions. *Crystals* **2017**, *7*, 212. [CrossRef]
42. Bondi, A. van der Waals Volumes and Radii. *J. Phys. Chem. A* **1964**, *68*, 441–451. [CrossRef]
43. Hohenstein, E.G.; Duan, J.; Sherrill, C.D. Origin of the Surprising Enhancement of Electrostatic Energies by Electron-Donating Substituents in Substituted Sandwich Benzene Dimers. *J. Am. Chem. Soc.* **2011**, *133*, 13244–13247. [CrossRef] [PubMed]
44. Yu, Y.; Rebek, J., Jr. Confined Molecules: Experiment Meets Theory in Small Spaces. *Q. Rev. Biophys.* **2020**, *53*, e6. [CrossRef] [PubMed]
45. Rahman, F.-U.; Tzeli, D.; Petsalakis, I.D.; Theodorakopoulos, G.; Ballester, P.; Rebek, J., Jr.; Yu, Y. Chalcogen Bonding and Hydrophobic Effects Force Molecules into Small Spaces. *J. Am. Chem. Soc.* **2020**, *142*, 5876–5883. [CrossRef] [PubMed]
46. Lide, D.R. (Ed.) *Handbook of Chemistry and Physics*, 87th ed.; CRC: Boca Raton, FL, USA, 2006.